Journal of Power Sources 271 (2014) 223–230

Contents lists available at ScienceDirect

Journal of Power Sources

journal homepage: www.elsevier.com/locate/jpowsour

Optimized electrochemical performance of three-dimensional porous $LiFePO_4$/C microspheres via microwave irradiation assisted synthesis

Feng Yu, San Hua Lim, Yongda Zhen, Yongxin An, Jianyi Lin*

*Institute of Chemical and Engineering Sciences (ICES), Agency for Science, Technology and Research (A*STAR), Singapore 627833, Singapore*

HIGHLIGHTS

- Microwave irradiation assisted synthesis (MIAS) heats precursor volumely and quickly.
- $LiFePO_4$/C (MIAS) effectively optimizes polarization performance at high charge/discharge rates.
- $LiFePO_4$/C (MIAS) exhibits excellent discharge potential voltage and specific energy.

GRAPHICAL ABSTRACT

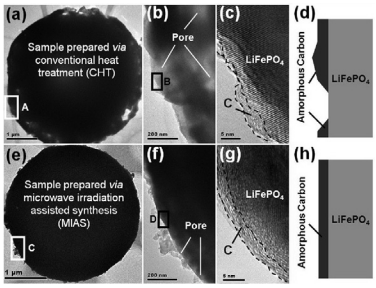

ARTICLE INFO

Article history:
Received 18 June 2014
Received in revised form
1 August 2014
Accepted 2 August 2014
Available online 10 August 2014

Keywords:
Lithium ion phosphate
Microwave irradiation
Porous microspheres
Polarization
Cathode material
Lithium ion batteries

ABSTRACT

Microwave irradiation assisted synthesis (MIAS) is successfully employed to prepare three-dimensional (3D) porous microspherical aggregation of $LiFePO_4$/C nanoparticles as the cathode material of lithium ion battery. XRD, SEM, and TEM studies confirm that highly crystalline $LiFePO_4$ without any impurity phase can be synthesized under microwave irradiation of 700 W for 5 min. The as-obtained $LiFePO_4$/C sample is prepared via MIAS consisting of nanopores (20–30 nm) and nanoparticles (20–30 nm) which are coated with uniform, complete carbon layers (about ~3 nm). These superior physical characters provide $LiFePO_4$/C (MIAS) excellent electrochemical performance at 0.1C including the high discharge capacity of 156.9 mAh g^{-1} and the low polarization of 51.5 mV. At the discharge rate of 1C, $LiFePO_4$/C (MIAS) exhibits the low polarization of 202.3 mV, high capacity of 126.7 mAh g^{-1}, high discharge voltage of 3.33 V, and specific energy of 398.5 kWh kg^{-1}, all of which are much better than those measured for the sample prepared via conventional heat treatment (CHT). At even high rate of 5C, $LiFePO_4$/C (CHT) fails to discharge whereas $LiFePO_4$/C (MIAS) is able to deliver the discharge capacity of 95.5 mAh g^{-1}. The low polarization of $LiFePO_4$/C (MIAS) results in the good discharge voltage of 3.06 V, high specific energy of 278.8 Wh kg^{-1}, and excellent energy efficiency of 72.0% at 5C.

1. Introduction

As one of the most promising cathode materials in lithium ion batteries (LIBs), olivine-structured $LiFePO_4$ has recently attracted significant attention since the groundbreaking work was conducted by Goodenough and his co-workers in 1997. [1,2] Compared with other cathode materials, such as olivine-structured $LiMPO_4$ (M = Mn, Co and Ni) , α-$NaFeO_2$ layered $LiMO_2$ (M = Co, Ni and

* Corresponding author. Institute of Chemical and Engineering Sciences (ICES), Agency for Science, Technology and Research (A*STAR), 1 Pesek Road, Jurong Island, Singapore 627833, Singapore. Tel.: +65 6796 3807 GMT+8h; fax: 65 6316 6182.
E-mail addresses: yufeng05@mail.ipc.ac.cn (F. Yu), lin_jianyi@ices.a-star.edu.sg (J. Lin).

http://dx.doi.org/10.1016/j.jpowsour.2014.08.009
0378-7753/

Mn), monoclinic structured $Li_{1+x}V_3O_8$, orthogonal structured Li_2MSiO_4 (M = Fe, Mn) , spinel structured $LiMn_2O_4$, NASCION structured $Li_3V_2(PO_4)_3$, *etc.*, $LiFePO_4$ not only exhibits innate electrochemical performance including a high theoretical capacity of 170 mAh g^{-1} and an acceptable operating voltage of 3.45 V (vs. Li^+/Li), but also shows advantages ideally suited for reversible electrochemical energy storage (EES) devices, such as thermal stability, long cycle life, low toxicity, low cost and environmentally benign processing. [3–5] These superiorities make $LiFePO_4$ play increasing roles in LIBs for electric vehicles (EVs) and load leveling systems for smart grids [6,7].

Although, the successfully commercialized $LiFePO_4$ as the cathode material for LIB is well positioned to meet demands of modern energy technology and consumer electronics, [8] it is still facing challenges, in particular for high-rate electrochemical performance. Generally, $LiFePO_4$ shows large polarization and low operating discharge voltage due to the slow Li-ion diffusion and low electron conductivity in $LiFePO_4$ [9] The polarization behaviors strongly affect the energy density of LIBs, in particular when LIBs are applied at high rates, and should be mitigated [10,11].

$LiFePO_4$ can be synthesized either via solid state or liquid-based route. In either case heat treatment is required and is undoubtedly a crucial process for improving the crystallinity of $LiFePO_4$ and mitigating the polarization effects. [12] Usually, traditional calcination is employed in heat treatment of $LiFePO_4$ precursors, no matter the precursors are prepared by ball milling, [13] sol–gel method, [14] co-precipitation, [15] solvothermal process, [16] or spray drying. [17] A way to follow the amorphous-to-crystalline transformation of $LiFePO_4$ material can be gained by using XAFS spectroscopy. [18] In this conventional heat treatment (CHT), energy is always transferred through heat convection, heat conduction and heat radiation from the surfaces to inners. CHT is both energy and time intensive process. Relatively high calcinations temperatures (e.g., 700 °C), which must be higher than the synthetic temperature of $LiFePO_4$/C and entail high energy power, and long heating period (a few to ten hours) are generally employed. [19–21] This is true particularly for a spray-drying process where spray drying is used to produce porous microspherical $LiFePO_4$/C nanocomposites. [17] To evaporate large amount of solvent, long time calcinations at high temperatures are required. Furthermore, CHT can easily carry a high risk of uneven crystallites and incomplete carbon coating for $LiFePO_4$/C composites, which is seriously inimical to Li-ion diffusion and unfavorable to reducing polarization and improving high rate performance [22,23].

Herein, we applied microwave irradiation assisted synthesis (MIAS) method in couple with spray-drying to prepare three-dimensional (3D) porous $LiFePO_4$/C microspheres. It is worthwhile to note that during MIAS the precursor compounds can be heated and reduced volumely by the quick, uniform and energy efficient microwave irradiation process. [24] MIAS method not only is an ideal heat treatment for economic, efficient and large-scale synthesis of electrode materials, it also helps to optimize physical characters, improve Li-ion diffusion kinetics, and reduce polarization, giving excellent high-rate electrochemical performance of $LiFePO_4$ [25,26].

2. Experimental

2.1. $LiFePO_4$/C powders preparation

Stoichiometric amounts of Li_2CO_3(AR), $Fe(NO_3)_3 \cdot 9H_2O$(AR), and $NH_4H_2PO_4$(AR) were dissolved in distilled water in molar ratio of n_{Li}:n_{Fe}:n_P = 1:1:1 and made into precursor liquid. P123, $HO(CH_2CH_2O)_{20}(CH_2CH(CH_3)O)_{70}(CH_2CH_2O)_{20}H$, which was a triblock copolymer used as soft template and carbon source in the present work, was added in the precursor liquid. The obtained liquid was spray dried in a spray dryer unit at a rate of 10 mL min^{-1} with inlet and outlet temperatures kept at 200 °C and 110 °C respectively. The spray dried precursor was then sintered in a tube furnace, heated at 10 °C min^{-1} in flowing argon atmosphere until 700 °C and held for 5 h to obtain CHT sample of $LiFePO_4$/C composite, which was marked LFPa. Another $LiFePO_4$/C sample which was marked LFPb was prepared via MIAS in a commercial microwave oven under microwave irradiation with 700 W for 5 min.

2.2. Physical characterization of the synthesized powders

Scanning electron microscopy (SEM) was performed on a JEOL JSM-7600F scanning electron microscope. Transmission electron microscopy (TEM) and high-resolution TEM (HRTEM) images were obtained with a Philips Tecnai-F20 transmission electron microscope. X-ray diffraction (XRD) analysis was carried out on a Bruker D8 Advance X-ray diffractometer with Cu Kα radiation (λ = 1.5406 Å). Brunauer–Emmett–Teller (BET) specific surface area and Barrett–Joyner–Halenda (BJH) pore structure were determined at 77 K by a N_2 adsorption-desorption method using a Micromeritics ASAP 2420 BET apparatus. The elemental analysis of total carbon was performed using a CHNS elemental analyzer Elementar Vario Micro Cube.

2.3. Electrochemical measurement

To fabricate the cathode of a coin cell battery, the as-obtained $LiFePO_4$/C composite was mixed with acetylene black and polyvinylidene fluoride (PVDF) in a weight ratio of 80:10:10 in *N*-methyl-2 pyrrolidinone (NMP). The obtained slurry was coated onto Al foil, dried at 120 °C for 12 h, and then punched into round plates with diameter of 12.0 mm as the cathode electrodes. Finally, the prepared cathode, a Celgard2400 separator (diameter of 16.0 mm), a lithium anode, electrolyte of 1 M $LiPF_6$ in EC-PC-EMC (1:1:3 vol.%), and the other components of the coin-type cell were assembled into a coin cell (CR2032) in an argon filled glove box (H_2O and O_2 < 1 ppm). The coin cells prepared were retained at room temperature for ten minutes at 4.2 V in charging and examined on a Maccor Series 4200 standard battery test system at various charge/discharge rates between 2.0 and 4.2 V. Electrochemical impedance spectroscopy (EIS) was performed using Solartron SI 1260 Impedance/Gain-Phase Analyser. The sinusoidal excitation voltage applied to the cells was 10 mV with a frequency range of between 1 MHz and 10 mHz.

3. Results and discussion

Crystallinity and phase information for the as-obtained samples were studied with X-ray powder diffraction (XRD) method. As shown in Fig. 1 all the diffraction lines in both LFPa and LFPb can be attributed to the orthorhombic phase $LiFePO_4$ (triphylite) (JCPDS card no. 40-1499) without any impurity phase. The profiles of the reflection peaks are quite narrow and symmetric, indicating the high crystallinity of the $LiFePO_4$ samples. Although the result of the element analysis confirms the presence of carbon, the carbon is not detectable in the XRD patterns since the residual carbon is amorphous. The calculated absolute lattice parameters of the as-obtained samples, using a space group of Pnma as the refinement model, are close to the corresponding of PDF value and similar to the previous reports (Table 1), [1] indicating that the perfect olivine phase $LiFePO_4$ could be prepared by MIAS (microwave irradiation 700 W, 5 min) as well as CHT (700 °C, 5 h). The calculated grain size is 54 nm for LFPb vs. 75 nm for LFPa (Table 2), using the

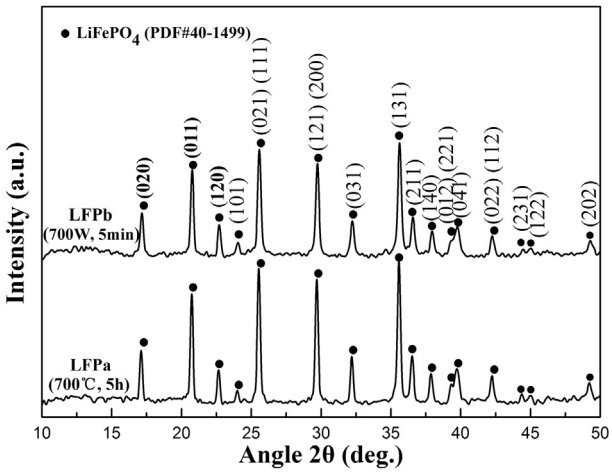

Fig. 1. XRD patterns of the as-obtained $LiFePO_4$/C samples LFPa prepared via conventional heat treatment of 700 °C for 5 h and LFPb prepared via microwave irradiation assisted heat treatment of 700 W for 5 min, respectively.

Debye–Scherrer equation and five crystal lattice indexes of (011), (111), (121), (031) and (131).

Scanning electron microscopy (SEM) images of the as-obtained samples LFPa and LFPb are shown in Fig. 2. 3D porous $LiFePO_4$/C microspheres with micro-nano-structures are successfully obtained largely due to triblock copolymer P123. Dissolved P123 forms micelles that can be used as the backbone to make structured mesoporous $LiFePO_4$/C when they are self-assembled into the $LiFePO_4$ precursor and then converted to carbon coating through carbonization [27,28]. It is noted that dissilient $LiFePO_4$/C microspheres were obtained perhaps due to slow thermal conductivity in CHT (Fig. 2a and c), while microwave irradiation provided uniform and instant heating, resulting in the uniformly distributed fine pores in the $LiFePO_4$/C microspheres (Fig. 2b and d). Correspondingly, the as-obtained samples LFPa and LFPb gave the BET specific surface area of 19.1 $m^2\ g^{-1}$ and 14.2 $m^2\ g^{-1}$, BJH adsorption average pore diameter 20.5 nm of and 24.3 nm, respectively (Fig. 2e and f). Transmission electron microscopy (TEM) observation of a single microsphere further confirms that sample LFPa consists of submicron-scale $LiFePO_4$/C micro-nano particles and pores (see Fig. 3a and b). Sample LFPb also exhibits micro-nanopores on the surface of $LiFePO_4$/C microsphere because of undissilient phenomenon happened to $LiFePO_4$/C microspheres in MIAS process (Fig. 3e and f). Thus TEM observations indicated that both LFPa and LFPb consisted of 3D porous $LiFePO_4$/C microspheres with micro-nano-structures, in agreement with the SEM result. These 3D porous $LiFePO_4$/C microspheres with nanoparticles and nanopores are strongly in favor of Li-ion diffusion and efficient contact between active materials and electrolytes [29,30].

In order to further examine the morphology and microstructure details of the as-obtained title product superstructures, high-resolution TEM (HRTEM) analysis was employed to reveal the fine superstructures of the samples LFPa and LFPb. As shown in Fig. 3c and g, the clear lattice image demonstrates the high crystallinity

Table 1
Comparison of lattice parameters of various $LiFePO_4$/C samples.

Samples	*a* axis/Å	*b* axis/Å	*c* axis/Å	Volume/$Å^3$
LFPa	6.010	10.338	4.697	291.83
LFPb	6.012	10.316	4.697	291.28
Padhi et al. [1]	6.008	10.334	4.693	291.39
JCPDS 40-1499	6.019	10.347	4.704	292.95

Table 2
Residual carbon content, BET specific surface area, BJH pore diameter and calculated grain size of the as-obtained $LiFePO_4$/C samples, LFPa (CHT) and LFPb (MIAS).

Samples	Heat treatment	Residual carbon content (wt.%)	BET surface area ($m^2\ g^{-1}$)	BJH pore diameter (nm)	Calculated grain size (nm)
LFPa	Calcination (700 °C, 5 h)	2.42	19.1	20.5	75.1
LFPb	Microwave (700 W, 5 min)	3.23	14.2	24.3	54.4

single-crystal features of the $LiFePO_4$/C superstructures, which is in good agreement with the XRD results. An amorphous carbon layer can be clearly seen, covering the surface of $LiFePO_4$. Compared with uncompleted carbon layer of the sample LFPa, the carbon coating layer on LFPb is uniform and completed, with a thickness of 2~3 nm and carbon content of 3.2 wt.% (Table 2). It is clearly demonstrates that the microwave irradiation can provide an "inert and instant heating" rather than the slow heat transfer from surface to bulk in conventional heating treatment. It is worth mentioning that carbon coating plays crucial role in improving the performance of $LiFePO_4$. Incomplete covering of the entire $LiFePO_4$ surface can easily lead to a noncontinuous and insufficient conducting network. Thanks to the "inert and instant heating" provided by microwave irradiation, LFPb exhibited uniform carbon coating and hence gave the sufficient electronically conducting network, which are contributed to the excellent electrochemical performance of $LiFePO_4$ [23,31].

To understand the formation mechanism of 3D porous microspherical aggregates of $LiFePO_4$/C nanocomposites prepared via different heat treatment routes, a schematic illustration is proposed in Fig. 4. The microspherical $LiFePO_4$/C aggregation mainly consists of three steps: (1) preparation of $LiFePO_4$/C precursor solution; (2) Spray drying; and (3) Heat treatment. Firstly, as the template and carbon source, P123 (i.e., $EO_{20}PO_{70}EO_{20}$, where EO stands for ethylene oxide and PO stands for propylene oxide) is added into $LiFePO_4$ precursor solution, forming $LiFePO_4$/C precursor solution. P123 behaves similarly to those of hydrocarbon surfactants, and can form spherical micelles in water, that can be used as the backbone/soft template to make mesoporous structure. P123 is uniformly distributed in the $LiFePO_4$ precursor aggregation. Secondly, in spray drying process the precursor microspherical aggregation is formed due to fast water evaporation of droplets. Finally, during heat treatment process homogeneous pores are formed from P123 degradation and carbonization when the precursor is heat treated. Meanwhile, the carbon from the P123 provides a special environment favorable for the reduction of Fe(III) and the formation of 3D porous microspherical aggregations of $LiFePO_4$/C nanocrystalline composite material. Different from the heat treatment of traditional calcination, microwave irradiation can provide "inert and instant heating" which can effectively avoid dissilient $LiFePO_4$/C microspheres and quickly form the uniformly fine pores on the surface of and inside $LiFePO_4$/C microspheres.

Electrochemical characterization of the as-obtained samples LFPa and LFPb are shown in Fig. 5a and b. The specific discharge capacities of LFPa and LFPb are 143.2 mAh g^{-1} and 156.9 mAh g^{-1} respectively at 0.1C. Both the charge–discharge profiles exhibit the voltage plateaus indicative of a typical $LiFePO_4$. [1] With increasing current rates, both samples present smaller reversible capacity and lower discharge voltage due to the rise of electrode polarization, which leads to increased separation of charge/discharge plateaus. [35] At the rate of 1C, the as-obtained samples LFPa and LFPb deliver discharge capacity of 75.6 mAh g^{-1} and 126.7 mAh g^{-1} respectively, which is 52.3% (LFPa) and 80.7% (LFPb) of the maximum capacity at 0.1C, respectively. The results show that LFPb

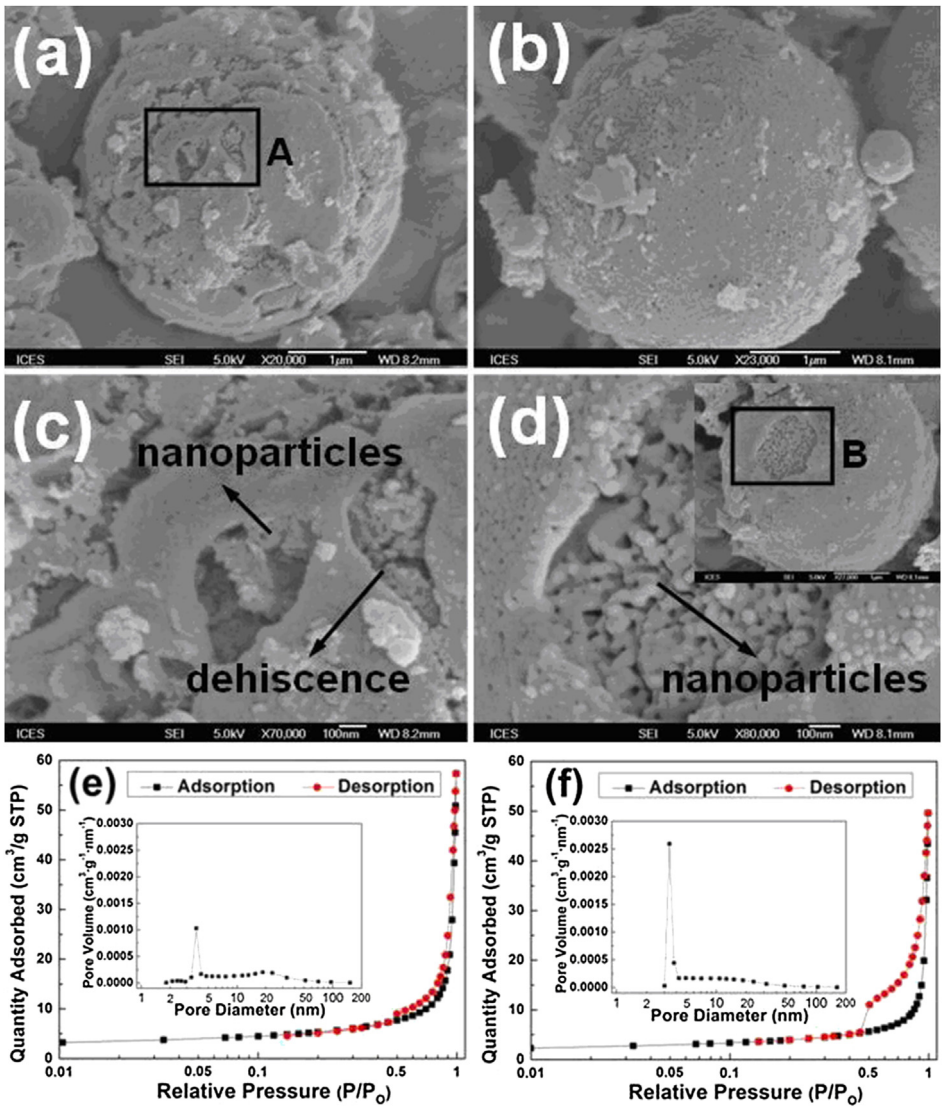

Fig. 2. Morphological characteristics of the as-obtained $LiFePO_4$/C samples LFPa and LFPb. (a, b) SEM images of individual $LiFePO_4$/C microsphere; (c) an enlarged SEM image of area A (indicated by a rectangle in panel a); (d) an enlarged SEM image of area B (inset); (e, f) nitrogen adsorption-desorption isotherms at 77 K and pore size distribution (inset) for the as-obtained samples LFPa and LFPb respectively.

performed better special capacity and capacity retention than LFPa. It can be clearly seen from Fig. 5a and b that LFPa possesses larger polarization than LFPb. As the charge–discharge rate was moved up to 2C, LFPa exhibited no discharge capacity and no voltage plateau due to the large polarization when it was cycled in the voltage of 2.0–4.2 V. However, LFPb can still deliver discharge capacities of 115.3 mAh g^{-1} at 2C, which confirm excellent rate capabilities with 73.5% of the maximum capacity (156.9 mAh g^{-1} at 0.1C). Even at the rate as high as 5C and 10C, the reversible capacity of 95.5 mAh g^{-1} and 73.5 mAh g^{-1} can be achieved respectively. The good rate capability may be due to its small polarization so that $LiFePO_4$/C of LFPb shows high specific capacity as it is discharged with high C rates.

To further compare the polarization effect of LFPa and LFPb, i.e. the voltage gap between the charge and discharge plateaus, we employed different capacity (dQ/dV) versus potential (V) of Li/$LiFePO_4$ cells cycled at various rates. As shown in Fig. 5c, two polarization peaks of each sample are observed in voltage region of 2.0–4.2 V at 0.1C. These two polarization peaks corresponding to oxidation and reduction potentials are directly observed to provide the voltage value of phase transition between $LiFePO_4$ and $FePO_4$ [32–34]. The as-obtained LFPb exhibits the dQ/dV potential of oxidation plateau peak at 3.46 V during charging indicating the phase transition of $LiFePO_4$ to $FePO_4$. The corresponding reduction peak of LFPb is at 3.40 V during discharging, indicating the phase transition of $FePO_4$ back to $LiFePO_4$. In comparison the charge/discharge peaks of LFPa are located at 3.52 and 3.33 V respectively. Obviously, the polarization, i.e. the voltage difference between charging and discharging potentials is much larger for LFPa vs. LFPb (183 mV vs. 51.5 mV at 0.1C), indicating that the kinetics of the $LiFePO_4$ is indeed improved with the heat treatment of microwave irradiation. The less in the potential difference between oxidation and reduction peaks, the better in reversibility of redox reaction. [35,36] Fig. 5d shows the polarization of the as-obtained samples LFPa and LFPb at various rates. LFPb possesses much smaller polarization of 203.3 mV resulting in the discharge plateau of 3.33 V at the rate of 1C while LFPa exhibits larger polarization of 1655.5 mV resulting in the low discharge plateau of 2.52 V.

It is notable that the large polarization not only decreases the potential discharge voltage, but also decreases the specific energy

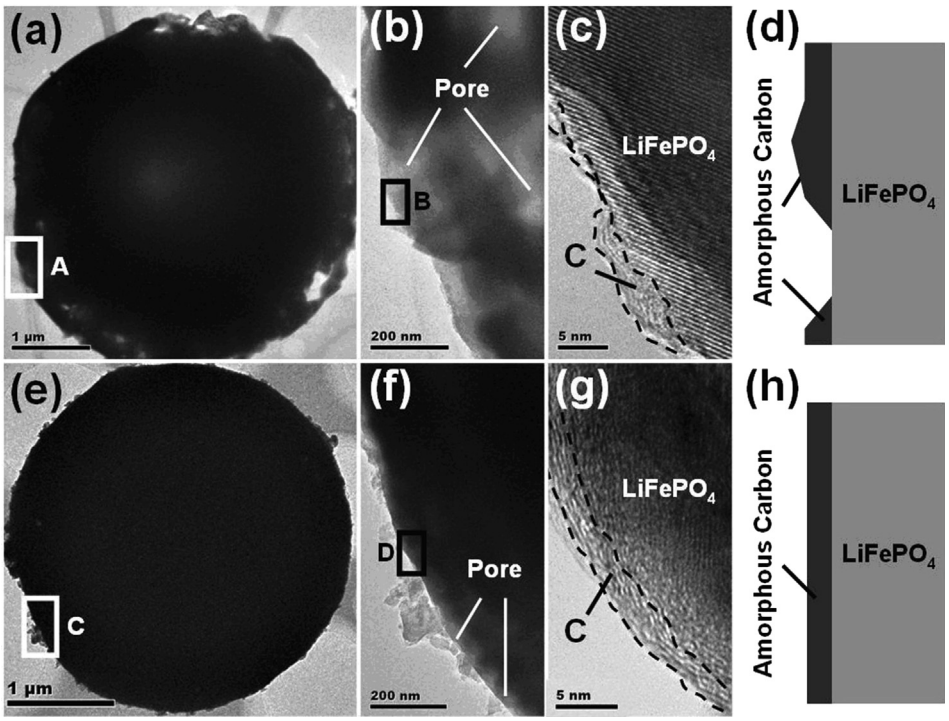

Fig. 3. TEM images of the as-obtained porous microsphere: Individual $LiFePO_4$/C microsphere for (a) LFPa and (e) LFPb; (b, f) enlarged TEM image of area A on LFPa (indicated by a rectangle in panel a), and area C on LFPb (indicated by a rectangle in panel b); (c, g) HRTEM images of areas B and D, as indicated by a rectangle in panel b (for LFPa) and f (for LFPb) respectively; (d, h) schematic structure of carbon coating layers on the surface of $LiFePO_4$/C microsphere: (d) non-uniform, incomplete amorphous carbon layer on LFPa, and (h) uniform, complete carbon layer on LFPb.

and energy efficiency. As shown in Fig. 5e and f, the specific discharge energy of the samples LFPa and LFPb are 463.2 Wh kg^{-1} and 512.7 Wh kg^{-1} respectively at 0.1C, with corresponding charge energy of 512.1 Wh kg^{-1} and 551.0 Wh kg^{-1} respectively for the cathode active material. The energy efficiency, i.e. the ratio of discharge/charge energies during the 0.1C cycle is about 90.5% for LFPa, which is lower than 93.0% for LFPb. With increasing polarization at 1C, LFPa only delivers the specific energy of 186.7 Wh/kg, while LFPb has the specific energy of 398.5 Wh kg^{-1}. At 1C the energy efficiency of LFPb is 87.3%, much larger than 59.0% of LFPa. At even higher rates, 5C and 10C, LFPb can perform with 270.8 Wh kg^{-1} and 188.6 Wh kg^{-1} respectively, whereas no discharge is possible at these high C rates for LFPa due to large potentials. All the results aforementioned indicate that LFPb exhibits better electrochemical performance than LFPa and MIAS is a better heat treatment method than CHT, in particular for high rate performance.

Overvoltages may be caused by concentration polarization and charge transfer polarization. In order to understand the internal resistances and polarization effects in the cell, electrochemical impedance spectroscopy (EIS) was employed. Fig. 6a shows the Nyquist plots of EIS for the as-obtained samples LFPa and LFPb, with the equivalent circuit being shown in the inset of Fig. 6b. The intercept at the Z' axis in high frequency end corresponds to the ohmic drop (R_e), which is related to the resistance of active materials, the current collectors and the material contacts such as electrolyte–electrode interface. The semicircle in the middle frequency range represents the charge transfer resistance (R_{ct}). The data collected in Table 3 show that both R_e and R_{ct} decrease in LFPb as compared to LFPa. This phenomenon may be due to homogeneous porous structure, uniform pore size distribution and complete thin carbon coating of the sample LFPb. The characteristic frequency peaks of LFPb in Bode phase plots as shown in Fig. 6c shifts to higher frequency as compared with that of LFPa, which may mean the electron transport is faster and the polarization resistance decreases in LFPb [37,38]. The results are consistent with the fact that the sample LFPb processes low polarization, good capacity and high rate performance. This observation implies that the microwave heating as a heat treatment route enables $LiFePO_4$ to possess a favorable structure and hence have lower ohmic resistance and faster charge transfer (than those in LFPa prepared via CHT).

In Fig. 6a, the slope of the inclined line in the low frequency region represents the Warburg impedance (Z_w), which is associated with Li-ion diffusion in the $LiFePO_4$ particles. The Li-ion diffusion coefficient D (in $cm^2\ s^{-1}$), which is considered to be the slowest process of charge transfer, can be calculated using the following equation [39]:

$$D = \frac{R^2T^2}{2n^4F^4A^2C^2\sigma^2} \quad (1)$$

$$Z'' = \sigma\omega^{-1/2} \quad (2)$$

where R is the universal gas constant, T is the absolute temperature (in K), n the number of moles of electrons transferred in the reaction ($n = 1$ for Fe^{3+}/Fe^{2+} redox pair), F the Faraday constant, A the area of the electrode (in cm^2), C the Li-ion concentration (i.e., 7.69×10^{-3} mol cm^{-3}), and σ the Warburg coefficient (in ohm $s^{1/2}$) which can be obtained by Equation (2). Fig. 6d shows the relationship between Z'' and square root of frequency $\omega^{-1/2}$ in the low frequency region, the value of σ can be obtained from the slop. The Li-ion diffusion coefficients of the sample LFPa and LFPb were calculated to be 3.68×10^{-14} $cm^2\ s^{-1}$, and 7.40×10^{-12} $cm^2\ s^{-1}$ respectively, which are comparable to those reported in literature,

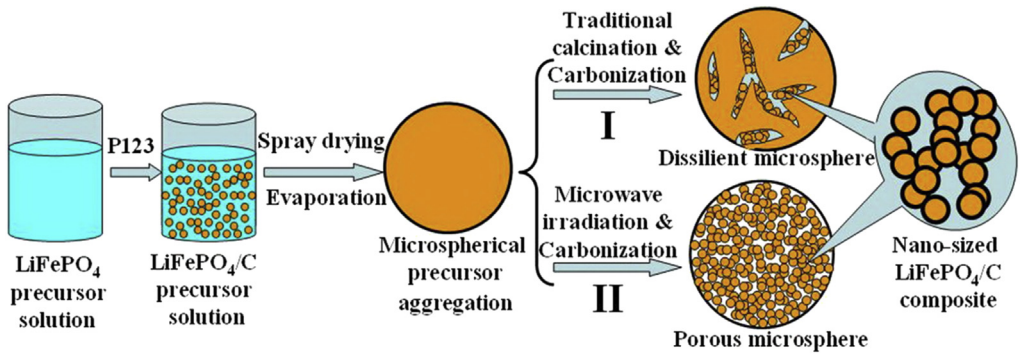

Fig. 4. Schematic illustration of 3D porous micro-nano-structured microspherical $LiFePO_4$/C aggregation via spray drying and subsequent heat treatment: (I) traditional calcination; (II) microwave irradiation heating.

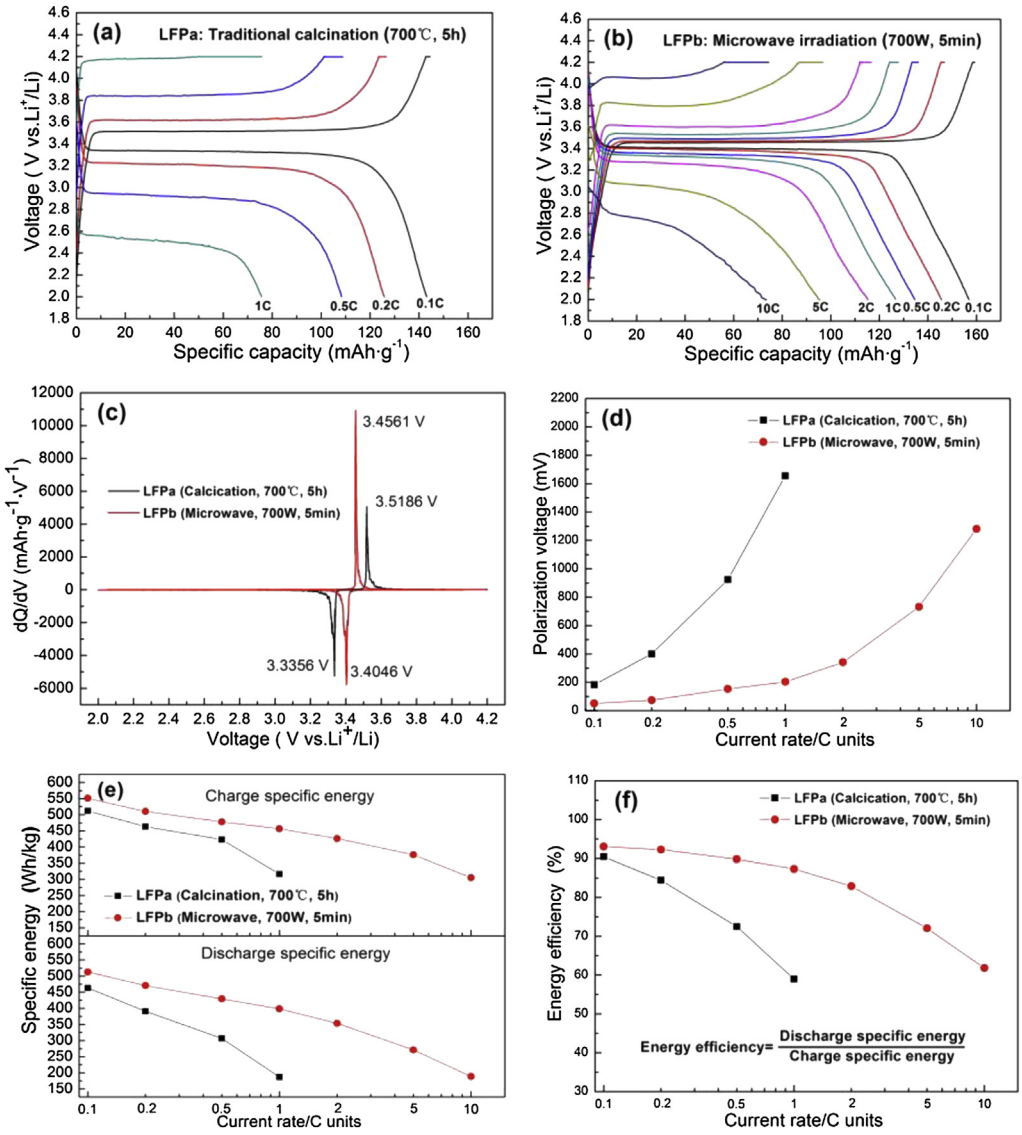

Fig. 5. Electrochemical performance of as-obtained $LiFePO_4$/C samples at different current densities in the potential window 2.0–4.2 V: (a, b) charge–discharge tests for LFPa and LFPb at various C rates between 0.1C and 10C respectively; (c) differential capacity (dQ/dV) as a function of potential (V) for the as-obtained samples LFPa and LFPb at 0.1C; (d) polarization voltage derived from the phase transition peaks of differential capacity (dQ/dV) as a function of potential (V) for LFPa and LFPb respectively at various C rates; (e) charge specific energy and discharge specific energy of LFPa and LFPb; (f) energy efficiency of LFPa and LFPb at various C rates, i.e. the ratio of discharge specific energy to charge specific energy.

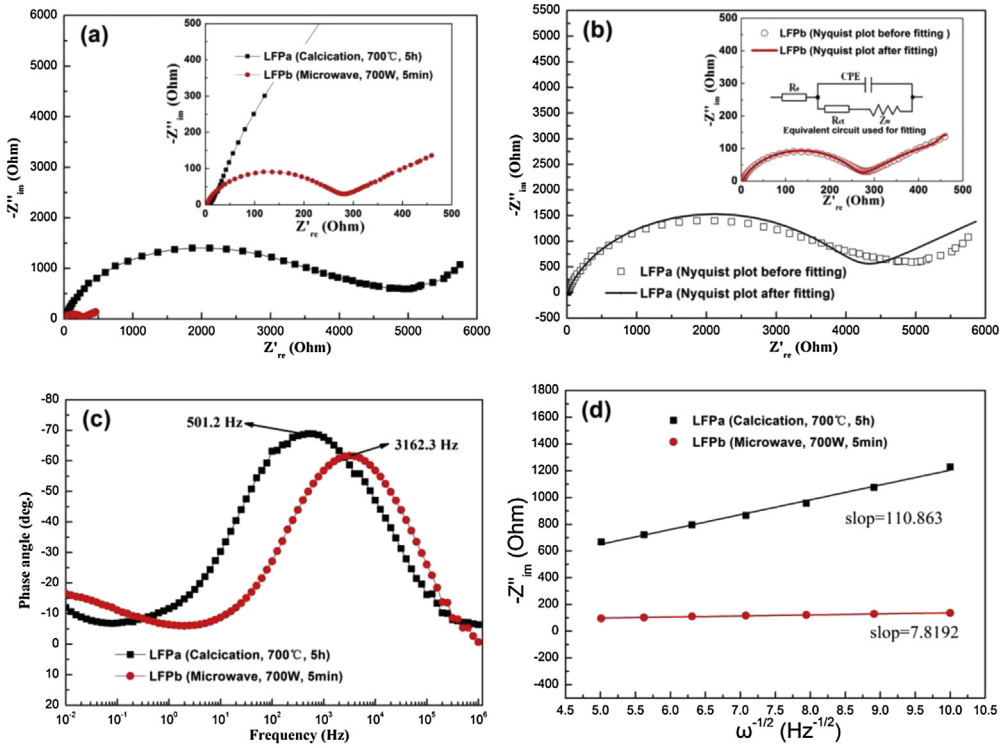

Fig. 6. Electrochemical impedance spectroscopy (EIS) measurements performed over a frequency range of 1 MHz–10 mHz at a charged stage with applied amplitude of 10 mV. (a) Electrochemical impedance diagram (Nyquist plot) for the as-obtained samples LFPa and LFPb; (b) Nyquist plot after fitting and the equivalent circuit used for fitting the experimental EIS data (inset); (c) Bode plot of phase angle verses frequency; (d) relationship between Z'' and square root of frequency ($\omega^{-1/2}$) in the low-frequency region.

such as 9.98×10^{-14} cm^2 s^{-1} for $LiFePO_4$/C, [40] 4.31×10^{-13} cm^2 s^{-1} for $LiFePO_4$/C, [41] 1.7×10^{-12} cm^2 s^{-1} for $LiFePO_4$/C, [42] 1.4×10^{-12} cm^2 s^{-1} for $LiFePO_4$/CNT. [43] Note that the real working surface of the electrode is much larger than the geometric surface, so that the calculation of the diffusion coefficient D based on geometric surface may lead to overestimating of the diffusion coefficient D. These results nevertheless indicate that the Li-ion diffusion has been drastically promoted in the sample LFPb, prepared via microwave irradiation assisted treatment. The decreased charge transfer resistance R_{ct} and the improved Li-ion diffusion in the sample LFPb are undoubtedly in favor of the excellent discharge capacities and superior rate characteristics in Fig. 5.

4. Conclusion

Microwave irradiation assisted synthesis (MIAS) in couple with spray-drying is an exceptionally good method to synthesize 3D porous micro-nano-structured $LiFePO_4$/C microspheres for the application in Li ion battery as cathode material. Compared with the energy and time intensive conventional heat treatment (CHT), MIAS method which can give "inert and instant heating" of $LiFePO_4$ precursors is an economic, efficient and environmentally benign material synthesis technique for LIBs. Furthermore, the $LiFePO_4$/C synthesized by MIAS method processes overwhelming structural superiorities including smaller crystallite size (54 nm), large BET surface area (14.2 m^2 g^{-1}), suitable pore structure (24.3 nm in diameter) and uniform complete carbon coating (3.2 wt.%), all of which are in favor of reducing polarization and improving electrochemical performance of $LiFePO_4$. Specifically, the as-obtained $LiFePO_4$/C (MIAS) sample processed high Li-ion diffusion (7.40×10^{-12} cm^2 s^{-1}) and low polarization (51.5 mV) at 0.1C. At high charge–discharge rates, the advantage of MIAS over CHT is even evident. At 1C, the $LiFePO_4$/C prepared via CHT method showed large polarization of 1655.5 mV and low capacity of 75.6 mAh g^{-1}, which resulted in the low discharge voltage of 2.52 V and small specific energy of 186.7 Wh kg^{-1}. On the other hand, the $LiFePO_4$/C prepared by MIAS gave low polarization of 203.3 mV and delivered high capacity of 126.7 mAh g^{-1}, resulting in high discharge voltage of 3.33 V, large specific energy of 398.5 Wh kg^{-1}, and high energy efficiency of 87.3%. At even high rate 5C, where $LiFePO_4$/C (CHT) failed to discharge due to the severe polarization, the as-obtained $LiFePO_4$/C (MIAS) could still perform high discharge voltage of 3.06 V and deliver the discharge capacity of 95.5 mAh g^{-1}, specific energy of 270.8 Wh kg^{-1} and energy efficiency of 72.0%. Certainly the MIAS method illuminates an efficient, cost-effective, and environmentally benign way to prepare the title product, which processes excellent electrochemical performance including low polarization, high discharge voltage, excellent specific energy, energy efficiency, *etc*. Additionally, the MIAS method holds the potential for the preparation of many other materials (such as $Li_4Ti_5O_{12}$ anode) for LIBs.

Table 3
Comparison of electrode kinetic parameters of as-obtained $LiFePO_4$/C samples.

Samples	R_e/Ω	R_{ct}/Ω	D/cm^2 s^{-1}
LFPa	8.45	4191.12	3.68×10^{-14}
LFPb	2.74	271.64	7.40×10^{-12}
Gao et al. [40]	8.74	106.78	4.31×10^{-13}

Acknowledgment

This work was financially supported by Agency for Science, Technology, and Research (A*STAR), Singapore for ACAR project ICES/11-513A01. We would also acknowledge GP Batteries

International Limited and King Powers Advanced Materials Co. Ltd, who provide collaborative supports to our works.

References

[1] A.K. Padhi, K.S. Nanjundaswamy, J.B. Goodenough, J. Electrochem. Soc. 144 (1997) 1188–1194.
[2] A.K. Padhi, K.S. Nanjundaswamy, C. Masquelier, S. Okada, J.B. Goodenough, J. Electrochem. Soc. 144 (1997) 1609–1613.
[3] M.S. Islam, C.A.J. Fisher, Chem. Soc. Rev. 43 (2014) 185–204.
[4] M.S. Whittingham, Chem. Rev. 104 (2004) 4271–4302.
[5] F. Yu, J.J. Zhang, C.Y. Wang, J. Yuan, Y.F. Yang, G.Z. Song, Prog. Chem. 22 (2010) 9–18.
[6] J.M. Tarascon, M. Armand, Nature 414 (2001) 359–367.
[7] R. Marom, S.F. Amalraj, N. Leifer, D. Jacob, D. Aurbach, J. Mater. Chem. 21 (2011) 9938–9954.
[8] K. Zaghib, A. Mauger, C.M. Julien, J. Solid State Electrochem. 16 (2012) 835–845.
[9] P.P. Prosini, M. Lisi, D. Zane, M. Pasquali, Solid State Ionics 148 (2002) 45–51.
[10] J.B. Goodenough, Y. Kim, Chem. Mater. 22 (2010) 587–603.
[11] D.W. Liu, G.Z. Cao, Energy Environ. Sci. 3 (2010) 1218–1237.
[12] O. Toprakci, H.A.K. Toprakci, L.W. Ji, X.W. Zhang, KONA Powder Part. J. (2010) 50–73.
[13] B. Kang, G. Ceder, Nature 458 (2009) 190–193.
[14] Y.G. Wang, Y.R. Wang, E.J. Hosono, K.X. Wang, H.S. Zhou, Angew. Chem. Int. Ed. 47 (2008) 7461–7465.
[15] H.M. Xie, R.S. Wang, J.R. Ying, L.Y. Zhang, A.F. Jalbout, H.Y. Yu, G.L. Yang, X.M. Pan, Z.M. Su, Adv. Mater. 18 (2006) 2609–2613.
[16] Y. Zhang, W.C. Wang, P.H. Li, Y.B. Fu, X.H. Ma, J. Power Sources 210 (2012) 47–53.
[17] F. Yu, J.J. Zhang, Y.F. Yang, G.Z. Song, J. Power Sources 195 (2010) 6873–6878.
[18] M. Giorgetti, M. Berrettoni, S. Scaccia, S. Passerini, Inorg. Chem. 45 (2006) 2750–2757.
[19] J.J. Chen, J. Graetz, ACS Appl. Mater. Interfaces 3 (2011) 1380–1384.
[20] Y.H. Yin, M.X. Gao, H.G. Pan, L.K. Shen, X. Ye, Y.F. Liu, P.S. Fedkiw, X.W. Zhang, J. Power Sources 199 (2012) 256–262.
[21] F. Yu, J.J. Zhang, Y.F. Yang, G.Z. Song, Electrochim. Acta 54 (2009) 7389–7395.
[22] G. Yang, Y. Kong, W. Hou, Q. Yan, J. Phys. Chem. B 109 (2005) 1371–1379.
[23] Y.S. Hu, Y.G. Guo, R. Dominko, M. Gaberscek, J. Jamnik, J. Maier, Adv. Mater. 19 (2007) 1963–1966.
[24] F. Yu, L. Zhang, M. Zhu, Y. An, L. Xia, X. Wang, B. Dai, Nano Energy 3 (2014) 64–79.
[25] A. Devadas, S. Baranton, T.W. Napporn, C. Coutanceau, J. Power Sources 196 (2011) 4044–4053.
[26] S. Balaji, D. Mutharasu, N. Sankara Subramanian, K. Ramanathan, Ionics 15 (2009) 765–777.
[27] N.N. Sinha, C. Shivakumara, N. Munichandraiah, ACS Appl. Mater. Interfaces 2 (2010) 2031–2038.
[28] F. Liang, Y.N. Dai, Y.C. Yao, Chin. J. Inorg. Chem. 26 (2010) 1675–1679.
[29] F. Yu, S.G. Ge, B. Li, G.Z. Sun, R.G. Mei, L.X. Zheng, Curr. Inorg. Chem. 2 (2012) 194–212.
[30] F. Yu, J.J. Zhang, Y.F. Yang, G.Z. Song, J. Mater. Chem. 19 (2009) 9121–9125.
[31] J.J. Wang, X.L. Sun, Energy Environ. Sci. 5 (2012) 5163–5185.
[32] H. Yu, H. Zhou, J. Mater. Chem. 22 (2012) 15507–15510.
[33] I. Belharouak, G.M. Koenig, J.W. Ma, D.P. Wang, K. Amine, Electrochem. Commun. 13 (2011) 232–236.
[34] J.S. Thorne, J.R. Dahn, M.N. Obrovac, R.A. Dunlap, J. Power Sources 216 (2012) 139–144.
[35] H. Gwon, H.-S. Kim, K.U. Lee, D.-H. Seo, Y.C. Park, Y.-S. Lee, B.T. Ahn, K. Kang, Energy Environ. Sci. 4 (2011) 1277–1283.
[36] H.-G. Jung, M.W. Jang, J. Hassoun, Y.-K. Sun, B. Scrosati, Nat. Commun. 2 (2011) 516.
[37] X. Dominguez-Benetton, S. Sevda, K. Vanbroekhoven, D. Pant, Chem. Soc. Rev. 41 (2012) 7228–7246.
[38] Z. He, F. Mansfeld, Energy Environ. Sci. 2 (2009) 215–219.
[39] A.J. Bard, L.R. Faulkner, 2nd ed., Wiley, N.Y., 2001, p. 231.
[40] H. Liu, Q. Cao, L.J. Fu, C. Li, Y.P. Wu, H.Q. Wu, Electrochem. Commun. 8 (2006) 1553–1557.
[41] F. Gao, Z.Y. Tang, Electrochim. Acta 53 (2008) 5071–5075.
[42] X.Z. Liao, Z.F. Ma, Q. Gong, Y.S. He, L. Pei, L.J. Zeng, Electrochem. Commun. 10 (2008) 691–694.
[43] Y.K. Zhou, J. Wang, Y.Y. Hu, R. O'Hayre, Z.P. Shao, Chem. Commun. 46 (2010) 7151–7153.